Polymer Testing 110 (2022) 107584

Contents lists available at ScienceDirect

Polymer Testing

journal homepage: www.elsevier.com/locate/polytest

Bone-targeted polymeric nanoparticles as alendronate carriers for potential osteoporosis treatment

Chunlan Jing [a,1], Shenmao Chen [b,1], Sehajdev Singh Bhatia [b,e], Bowen Li [a], Hongze Liang [a], Chaozong Liu [b,**], Zhenjiang Liang [c], Junying Liu [d], Haiyan Li [d], Ziyu Liu [b,***], Hui Tan [c,****], Lingling Zhao [a,b,*]

[a] Faculty of Materials Science and Chemical Engineering, Ningbo University, Ningbo, 315211, China
[b] Institute of Orthopaedic & Musculoskeletal Science, University College London, Royal National Orthopaedic Hospital, London, HA7 4LP, UK
[c] Pneumology Department, Shenzhen Children's Hospital, Shenzhen, 518026, China
[d] Department of Endocrinology, The First Affiliated Hospital, Shenzhen University, Shenzhen, 518035, China
[e] James Paget University Hospital, Gorleston, Great Yarmouth, NR31 6LA, UK

ARTICLE INFO

Keywords:
Osteoporosis
Nanoparticles
Bone-targeted
Alendronate

ABSTRACT

Bone-targeted polymeric nanoparticles for alendronate delivery based on Poly (lactic-co-glycolic acid) conjugated chitosan (CS-PLGA) and alendronate conjugated PLGA (Alen-PLGA) are fabricated and their superior performances are evaluated. The nanoparticles exhibited sustained Alen release without obvious burst release and good cytocompatibility against MC3T3 cells. Alen-modified nanoparticles demonstrated a high affinity to hydroxyapatite, which is the main mineral component of bone, indicating their feasibility for bone-targeted delivery. In addition, unlike nanoparticles without Alen, Alen-modified nanoparticles were preferentially taken up by MC3T3 cells, compared to HDF cells, revealing their specific uptake for osteoblast-like cells. Thus, the Alen-modified nanoparticles can potentially be developed as bone-targeted carriers for osteoporosis treatment.

1. Introduction

Osteoporosis is one of the most common metabolic disorders characterized by loss of bone mass and strength, which can significantly increase the potential of skeletal fractures and deterioration of bone microstructure, leading to serious secondary health problems and even death [1–4]. Current therapeutic approaches for osteoporosis treatment mainly rely on medication such as bisphosphonates (alendronate and zoledronate) and hormone (estrogen and calcitonin) [5–8]. Among them, alendronate (Alen) is an active molecule with well-proven efficacy indicated as first-line regimen for osteoporosis treatment [9,10]. Alen can prevent bone resorption and enhance the osteogenic differentiation [11,12]. However, the clinical use of Alen was limited due to its low oral bioavailability (only 0.7%) and numerous side effects related to the gastrointestinal tract [13].

Recently, multifunctional nanoparticles have been developed for the effective treatment of osteoporosis, and targeted drug delivery is considered a promising system to minimize the side effects and enhance the bioavailability [14–16]. For bone-targeted drug delivery, bisphosphonate, tetracycline and phytic acid are well-known functional ligands [17,18]. Among them, Alen is widely employed in the fabrication of bone-targeted drug carriers due to its high affinity to bone tissue as well as its therapeutic effects on bone diseases [19]. Ahn et al. developed Alen-conjugated nanodiamonds (Alen-NDs) as potential therapeutic agents for osteoporosis treatment [2]. Alen-NDs can reduce the proliferation rate of MC3T3-E1 cells without cell death, and change the cellular morphology from a fibroblastic shape to a cuboidal shape, demonstrating superior performance on osteogenic differentiation. Ye et al. synthesized bone-targeted near-infrared light and upconversion nanoparticles based on mesoporous-silica for the treatment of

* Corresponding author. Faculty of Materials Science and Chemical Engineering, Ningbo University, Ningbo, 315211, China.
** Corresponding author.
*** Corresponding author.
**** Corresponding author.
E-mail address: zhaolingling@nbu.edu.cn (L. Zhao).
[1] These authors contribute equally to this work.

https://doi.org/10.1016/j.polymertesting.2022.107584
Received 10 February 2022; Received in revised form 10 April 2022; Accepted 12 April 2022
Available online 15 April 2022

osteoporosis [5]. This nanoplatform showed reliable bone-targeting properties due to the Alen modification, and demonstrated a favorable curative effect of reversing osteoporosis due to the controllable release of NO in the bone tissue.

In this work, we designed Alen-modified nanoparticles based on CS-PLGA conjugate and Alen-conjugated PLGA (Alen-PLGA). Chitosan (CS) is a natural cationic polysaccharide with excellent biocompatibility and biodegradability, which has a variety of pharmaceutical uses and is widely used in drug delivery system [20,21]. On the other hand, Poly (lactic-co-glycolic acid) (PLGA) is one of the most widely used polymers for drug delivery in human and has been approved by United States-Food and Drug Administration, European Medicine Agency and other federal agencies, due to its biodegradability, biocompatibility and immune neutral properties [22,23]. Hence, CS-PLGA conjugate with merits of both CS and PLGA was synthesized for better drug delivery promises. Alen was selected as an anti-osteoporosis model drug as well as a bone-targeting ligand to modify PLGA. Thus, CS-PLGA/Alen-PLGA nanoparticles were prepared and their potential for bone-targeted delivery was evaluated.

2. Experimental part

2.1. Materials

PLGA (lactide:glycolide 75:25; M_W~9500, Dalian Meilun Biotechnology Co., Ltd), CS (75% deacetylation, M_W ~100 kDa, Ningbo Haixin Biological Co.), N-hydroxysuccinimide (NHS, Quzhou Xinteng Chemical Co., Ltd), alendronate (Alen, Hewns Technology Co., Ltd), N-Ethyl-N'-(3-dimethylaminopropyl) carbodiimide hydrochloride (EDC·HCl, Sinopharm Chemical Reagent Co., Ltd), fluorescein isothiocyanate isomer I (FITC, Macklin Biochemical Co., Ltd), nano hydroxyapatite (HAp, Macklin), Rhodamine B (RB, Shanghai Yuanye Bio-Technology Co., Ltd.).

2.2. Synthesis of PLGA conjugated CS (CS-PLGA)

The synthesis of CS-PLGA was according to our previous work [24]. Briefly, PLGA (0.2 g, 0.02 mmol), EDC·HCl (14.8 mg, 0.07 mmol) and NHS (6.1 mg, 0.053 mmol) were dissolved in 35 mL dimethyl sulfoxide and stirred at room temperature for 2 h. Then, the mixture was added to 0.2 g CS (1.24 mmol) dissolved in 10 mL acetum (10%) and stirred for another 24 h. Subsequently, the mixture was dialyzed against distilled water using a dialysis tube (MWCO: 8–14 kDa, Yuanye Bio-Technology Co., Ltd) for three days, and the residue was freeze-dried to harvest white cotton-like product (yield 89.4%). The degree of substitution (DS) of CS with PLGA was 1.92% determined using elemental analysis by comparing the carbon/nitrogen (C/N) molar ratio [25,26].

RB-labeled CS-PLGA (RB–CS–PLGA) was synthesized [27] for nanoparticle preparation in the cellular uptake and HAp affinity test. In brief, RB (16 mg, 0.0344 mmol), EDC (20.5 mg, 0.0107 mmol) and DMAP (0.9 mg, 0.0074 mmol) were dissolved in 4 mL distilled water and stirred of 0.5 h at 37 °C. Then, the mixture was added to CS-PLGA solution (160 mg dissolved in 16 mL 10% acetum) and stirred for another 24 h in dark. Subsequently, the reaction mixture was dialyzed against distilled water, and the residue was freeze-dried to harvest pink cotton-like product (yield 77.6%).

2.3. Synthesis of alendronate modified PLGA (Alen-PLGA)

The synthesis of Alen-PLGA was according to previous work [28]. Briefly, 32.5 mg Alen (0.1 mmol) was dissolved in 5 mL acetum (10%) and then freeze-dried to obtain acidulated Alen. PLGA (0.4 g, 0.04 mmol), EDC·HCl (29.6 mg, 0.155 mmol) and NHS (12.2 mg, 0.106 mmol) were dissolved in 4 mL dimethyl sulfoxide and dichloromethane mixed solution (v/v, 1:1) and stirred at room temperature for 2 h. To this, acidulated Alen dispersed in 1 mL dimethyl sulfoxide was added slowly under stirring. After another 24 h reaction, the dichloromethane was removed by rotary evaporation and then dialyzed against distilled water using a dialysis tube (MWCO: 3500 Da) for three days. The residue was freeze-dried to harvest white powder product (yield 86.9%).

2.4. Preparation of Alen-loaded nanoparticles

Nanoparticles was prepared according to a similar procedure reported [13], and FITC labeled Alen (FITC-Alen) (synthesized according to our previous work [24]) was used for quantitative analysis. In brief, 4.5 mg FITC-Alen dispersed in 1% PVA solution was added to a right amount of CS-PLGA solution (5 mg mL^{-1} in 10% acetum) and stirred under room temperature in dark for 10 min. Subsequently, PLGA-Alen solution (5 mg mL^{-1} in dichloromethane) was added to the CS-PLGA/FITC-Alen mixture and ultrasonicated for 15 min using an ultrasonic processor (JY92-IIN, power 25%). The dichloromethane was removed by rotary evaporation, and then the product was collected by centrifugation (12000 r/min) and washed using distilled water. The unloaded FITC-Alen in the supernatant was detected by fluorescence spectrophotometer. The loading content (LC) and loading efficiency (LE) of alendronate was calculated using the following formula:

$$LC(\%) = \frac{\textit{The fed amount of Alen} - \textit{The amount of Alen in supernatant}}{\textit{The amount of Alen} - \textit{loaded nanoparticles}} \times 100\%$$

$$LE(\%) = \frac{\textit{The fed amount of Alen} - \textit{The amount of Alen in supernatant}}{\textit{The fed amount of Alen}} \times 100\%$$

For empty nanoparticles without Alen-loading, PVA solution not containing FITC-Alen was used in the preparation process. For empty nanoparticles without Alen-decoration used in the HAp affinity test, PLGA instead of PLGA-Alen was used in the preparation process. Five different nanoparticle formulas were prepared by altering the feeding volume, as shown in Table 1.

2.5. Characterization

Infrared spectroscopy and ^1H NMR analysis of the synthesized sample were performed on Nicolet 6700 Fourier infrared spectrometer (Thermo Nicolet. USA) and Bruker AMX 400 MHz spectrometer (Bruker Swiss), respectively. The morphology, particulate size and surface charged of the prepared nanoparticles were detected by scanning electron microscopy (SEM) (Nova Nano SEM 450, FEI. USA) and Mastersizer (Malvern Zana ZS 90, US), respectively.

2.6. In vitro drug release

The drug release of Alen from nanoparticles was studied in vitro by dialysis method, and Phosphate Buffer Saline (PBS) at pH 7.4 was used as the release medium. Briefly, 3 mg Alen-loaded nanoparticles were dispersed in 1 mL PBS, and then transferred to a dialysis tube (MW 8–14 kDa). The dialysis tube was immersed into a brown vial containing 10 mL PBS and incubated at 37 °C in a thermostat water bath in dark. 2 mL of the release medium was taken out for fluorescence test at previous set timepoint, and 2 mL fresh PBS was supplemented to maintain the volume.

2.7. Cytotoxicity test

The cytotoxicity of the nanoparticles against MC3T3 cells was assessed by CCK-8 assay. In brief, 8×10^3 cells were seeded in 96-well plate, and 100 μL DMEM containing 10% fetal bovine serum was added. The cells were cultured in an incubator at 37 °C under 5% CO_2 for 24 h, and then the DMEM of each well was discarded and replaced with

Table 1
The formulations of 5 different nanoparticles.

Sample	Volume of CS-PLGA solution (mL)	Volume of Alen-PLGA solution (mL)	Volume of 1% PVA solution (mL)	Volume of RB–CS–PLGA solution (mL)	Volume of PLGA solution (mL)	Ratio of CS-PLGA to Alen-PLGA	Ratio of oil to water phase
NP1	2	1	1.5	–	–	2:1	2/7
NP2	1.5	1.5	3.75	–	–	1:1	2/7
NP3	1	2	6	–	–	1:2	2/7
NP4	0	1.5	3.75	1.5	–	1:1	2/7
NP5	0	–	3.75	1.5	1.5	1:1	2/7

equal volume of medium containing different concentration of nanoparticles (10–1000 μg mL^{-1}). After another 24 h of incubation, the culture medium was removed and the wells were washed gently using PBS three times. Subsequently, 100 μL DMEM containing 10 μL CCK-8 solution was added, and the optical density of each well was recorded using a microplate reader after 2 h incubation.

2.8. Cellular uptake

HDF and MC3T3 cells were applied in the cellular uptake test. 1×10^4 cells were seeded in 24-well plate and cultured in DMEM supplemented with 10% fetal bovine serum. After 24 h incubation, the culture medium was removed and replaced with equal volume of medium containing nanoparticles (50 μg mL^{-1}). At predetermined time (3 and 24 h), each well was washed gently using PBS to remove the nanoparticles that were not taken by cells. The amount of cellular uptake was quantitated using a similar method reported in previous [17]. 200 μL HCl was added to each well to solubilize the cells for 24 h, and then the solution was transferred to a 96-well plate for the measurement of nanoparticles using a microplate reader at 533 nm. The amount of cellular uptake was defined as the optical density of nanoparticles divided the number of cells (measured by CCK-8). In addition, HDF and MC3T3 cells treated with nanoparticles were washed three times with PBS and then fixed in 4% paraformaldehyde for 3 h. After washing three times with PBS, cell nuclei were stained with 4-6-diamidino-2-phenylindole (DAPI), and the cell morphology was observed under a Leica TCS SP5 II laser confocal microscope.

2.9. Affinity of nanoparticles to HAp

For the HAp affinity test, RB-labeled empty nanoparticles with or without Alen-decoration were used, and nano hydroxyapatites were compressed to Hap disks (d = 1 cm, 100 mg/disk). In brief, 4 mL nanoparticle dispersion (1 mg mL^{-1} in 0.9% NaCl) was added in a brown vial containing one HAp disk and incubated in dark under shaking for 0.5 h, 2 h and 18 h, respectively. The optical density of nanoparticle dispersion was recorded at 553 nm, and the binding ratio of nanoparticles to HAp was defined as the percentage of optical density reduction at 553 nm [24]. The HAp disks were washed using distilled water and then observed under a Leica TCS SP5 II laser confocal microscope.

2.10. Statistics

Statistical comparisons were accessed by variance analysis (ANOVA), and statistical significance was accepted at $p < 0.05$.

3. Results and discussion

3.1. Synthesis of CS-PLGA and Alen-PLGA

CS-PLGA and Alen-PLGA were synthesized though the amidation reaction between carboxyl group in PLGA and amino group in GC or Alen. The synthetic routes are illustrated in Scheme 1A and 1B, and the chemical structure was confirmed by FTIR and ^{1}H NMR spectrum. As shown in the FTIR spectrum of CS-PLGA (Fig. 1A), the broad absorption band between 3000 and 3600 cm^{-1} was due to O–H stretch superimposed on N–H stretch of CS, and the peaks at 1582 and 1645 cm^{-1} represented the vibration of amide I and amide II bands of CS [29,30]. The peak at 1746 cm^{-1} represented the presence of C═O group of amide [20,31]. In the ^{1}H NMR spectrum of CS-PLGA (Fig. 2A), the broad peak at approximately δ 3.6 was assigned to the protons on methoxy groups (–CH_2–O-) of the CS unit [32,33], and peaks at approximately δ 1.45 (overlapping doublets) indicated the methyl groups lactic units in PLGA, and multiplets at δ 4.8 and 5.2 were corresponded to the methylene groups of glycolic acid and methine groups of lactic acid residues, respectively [24,34]. All the results showed that PLGA was successfully conjugated to CS.

In the FTIR spectrum of Alen-PLGA (Fig. 1B), the peak at 3565 cm^{-1} was attributed to O–H stretch from Alen, and the broad absorption band at 3100-3450 cm^{-1} was assigned to N–H stretch of amide (–CO–NH) bond [6]. Compared to the spectrum of Alen, peaks at 1601 and 1645 cm^{-1} assigned to the N–H bend became much weaker in Alen-PLGA, suggesting the substitution of –NH_2 group in Alen and the conjugation of PLGA and Alen. Peaks at 2963 and 2877 cm^{-1} could be attributed to presence of C–H stretching, and the peak at 1746 cm^{-1} represented the presence of C═O group of amide, and the peak at 1078 cm^{-1} inferred the presence of C–O of PLGA [22]. The ^{1}H NMR spectrum of Alen was characterized mainly by two broad peaks at δ 3.0 and 2.0 (Fig. 2B), which were owing to the protons on methylene groups of –NH–CH_2- and –CH_2-CH_2-, respectively [6,28]. In the ^{1}H NMR spectrum of Alen-PLGA (Fig. 2C), the typical signals at approximately δ 1.45 (overlapping doublets) were owing to the methyl groups of lactic units in PLGA, and the multiplets at δ 4.8 were corresponding to the methylene groups of glycolic acid, and the peaks at approximately δ 5.2 were owing to the methine groups of lactic acid residues in PLGA [20,35]. In addition, the presence of Alen was confirmed by the small broad peaks at δ 3.2 and 2.2, indicating the successful synthesis of Alen-PLGA conjugation. Enlargement and integral of the diagnostic signals enabled calculation of the degree of substitution of Alen in the PLGA backbone, giving a mean conjugation yield of 49.6%.

3.2. Characterization of nanoparticles

Fig. 3A showed the SEM images of nanoparticles prepared by different feed ratios. The nanoparticles have regular spherical morphology with a diameter of 200–300 nm. Table 2 showed the hydrodynamic diameter and zeta potential of the nanoparticles. As shown in Fig. 3B, the nanoparticles had a Gaussian distribution in particle size, and the particles size had a slightly increase with the increase of Alen-PLGA ratio when the overall polymer amount was kept constant. The average size of nanoparticles was 209.7 ± 15.5, 237 ± 9.5 and 256.5 ± 4.6 nm for NP1, NP2 and NP3, respectively. The relative stability of nanoparticles was evaluated by incubating the nanoparticles in PBS for 82 h, and the particle sizes were measured using DLS at intervals. As shown in Fig. 3C, the particle size had a slight fluctuation during the

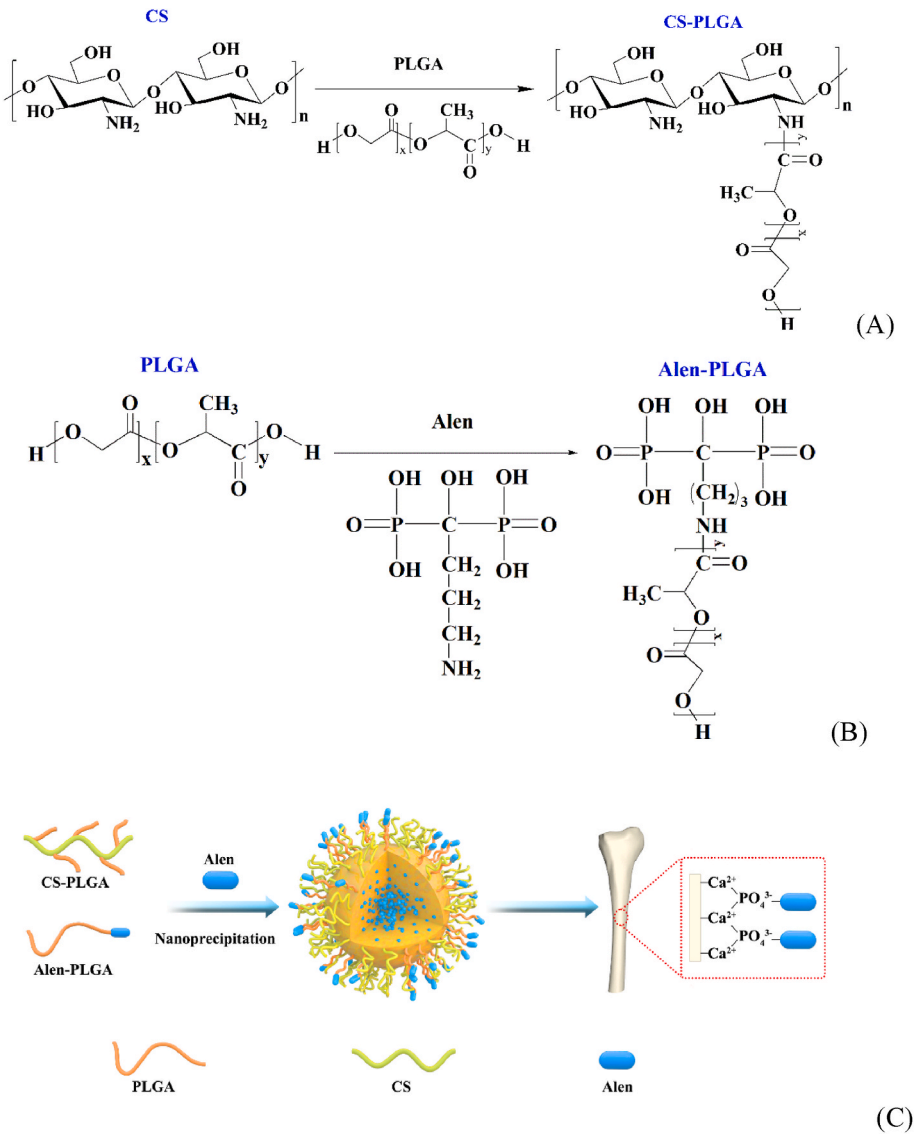

Scheme 1. Illustrative synthesis of CS-PLGA (A), Alen-PLGA (B), and Alen-modified nanoparticles for bone-targeted delivery (C).

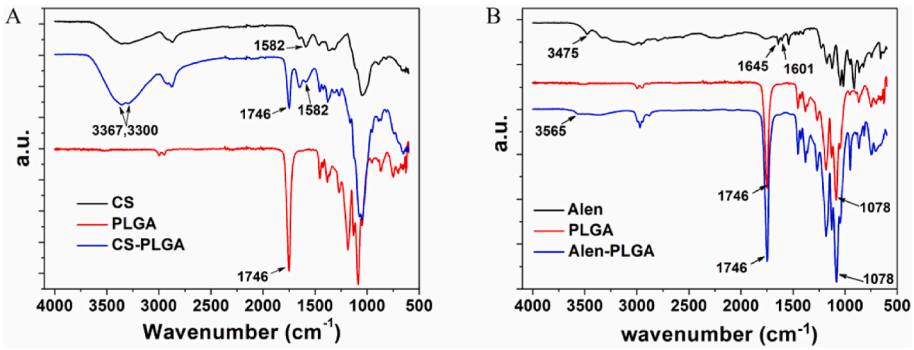

Fig. 1. (A) FTIR spectra of CS, PLGA and CS-PLGA. (B) FTIR spectra of Alen, PLGA and Alen-PLGA.

incubation time at room temperature, and this may be caused by the drug release and swelling of the polymeric nanoparticles. The surface charge of nanoparticles was indicated by zeta potential. The surface charge of the nanoparticles decreased with the increase of Alen-PLGA amount in the nanoparticles. As shown in Table 2, when the CS-PLGA/Alen-PLGA ratio was 2:1 (NP1) and 1:1(NP2), the nanoparticles had positively-charged surfaces, and when the ratio CS-PLGA/PLGA-Alen was 1:2 (NP3), the surface of nanoparticles was negatively charged. Since chitosan contributes positive charges to the nanoparticle due to the protonation of amino groups, and Alen contributes negative charges to the nanoparticle due to the ionization of phosphate groups, the negative charged surface of NP3 indicated that the bone-targeted

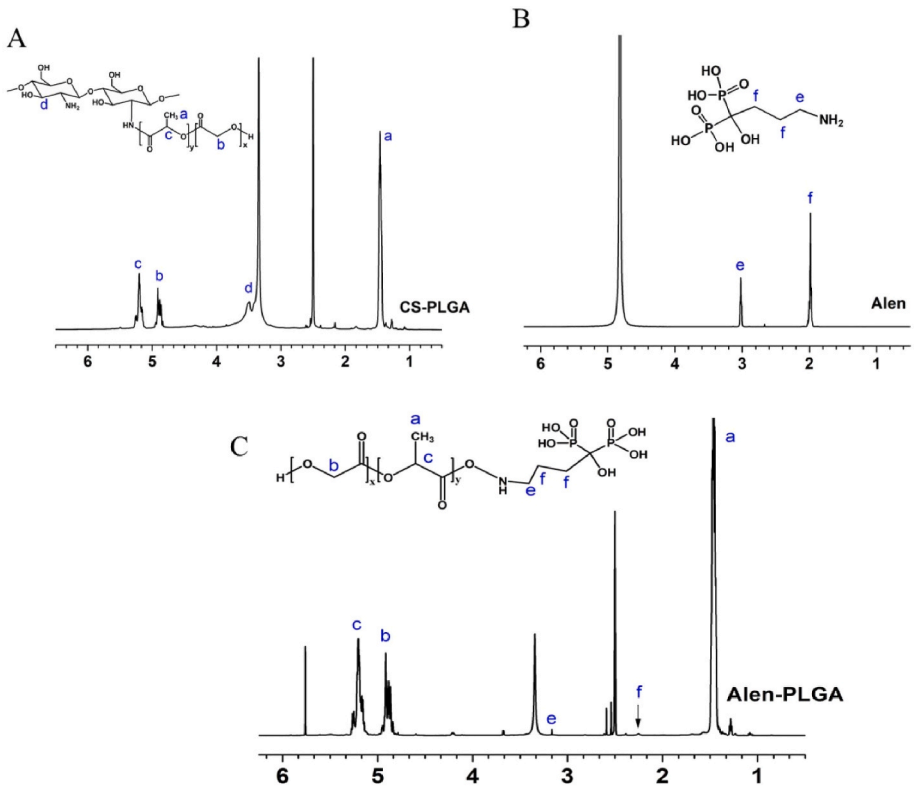

Fig. 2. ^{1}H NMR spectra of CS-PLGA (A), Alen (B) and Alen-PLGA (C).

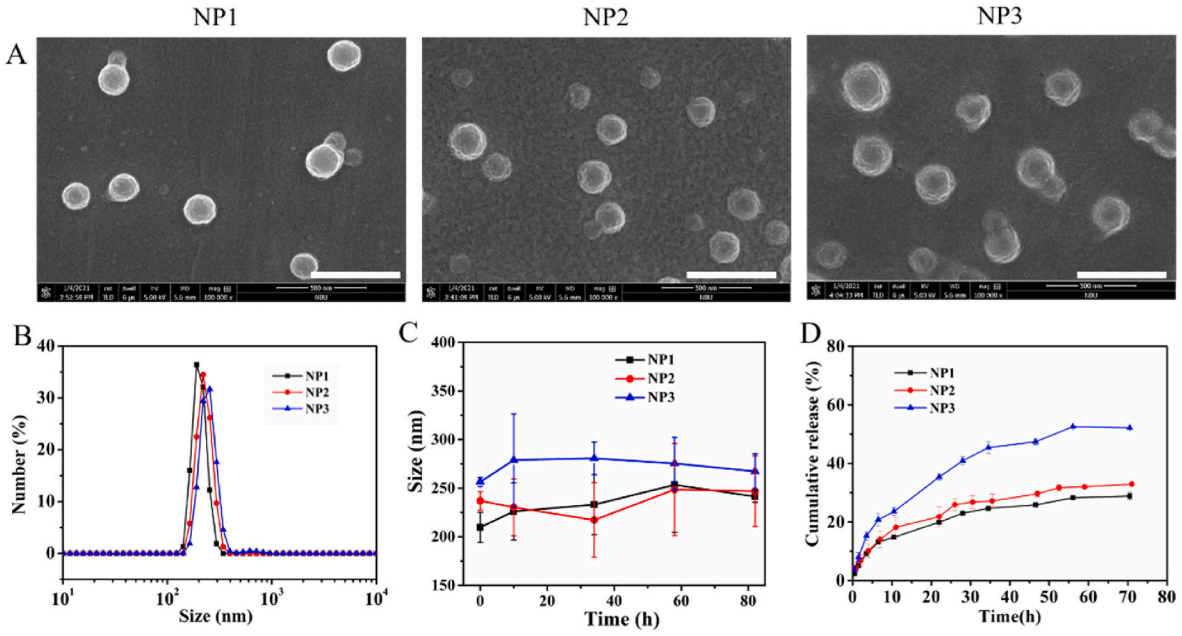

Fig. 3. (A) SEM images of nanoparticles with different polymer ratio. Size distribution (B), variation of particle size with time (C) and drug release profile (D) of different nanoparticles. Scale bar is 500 nm.

moiety (Alen) was partly distributed on the surface of nanoparticles, which is very important for the bone-targeting capability of nanoparticles.

3.3. *In vitro drug release*

As shown in Fig. 3D, Alen indicated sustained release from the nanoparticles without obvious initial burst release. Nanoparticles with different formulate had different release profile. The release rate of Alen increased with the increase amount of Alen-PLGA in the nanoparticles. Within 72 h of observation, 28.8, 32.9 and 52.2% of Alen was release from NP1, NP2 and NP3, respectively. The faster drug release of NP3 than that of NP2 and NP1 may be caused by the larger hydrodynamic diameter of NP3 than that of NP2 and NP1. The particles size increased

Table 2
Characterization of different nanoparticles.

Sample	Hydrodynamic diameter (nm)[a]	Zeta potential (mV)	LE (%)	LC (%)
NP1	209.7 ± 15.5	24.4 ± 0.5	77.2 ± 3.1	72.3 ± 5.8
NP2	237 ± 9.5	16.1 ± 3.5	71.3 ± 5.7	76.4 ± 10.3
NP3	256.5 ± 4.6	−2.64 ± 0.6	73.1 ± 7	74.4 ± 7.3
NP4	325.3 ± 6.1	−1.13 ± 0.4	–	–
NP5	334.9 ± 12.7	−1.87 ± 0.1	–	–

[a] Measured by DLS.

slightly with the increase of Alen-PLGA ratio when the overall polymer amount was kept constant (Fig. 3B), suggesting that NP3 has a looser structure than NP2 and NP1, thus facilitating the drug release. In addition, NP3 gave a larger hydrodynamic diameter than NP2 and NP1 during the incubation time in the particle stability test (Fig. 3C), indicating that the swelling degree of NP3 was larger than that of NP2 and NP1, which also resulted in the faster drug release. The drug release kinetics could be described using the Ritger-Peppas equation ($\frac{M_t}{M_\infty} = kt^n$), where M_t/M_∞ is the percentage of drug released at time t, and n is the diffusion correlation coefficient [13]. Results showed that these three nanoparticles formulation demonstrated similar release kinetics, and the calculated n values based on the release profile (Fig. 3D) were 0.39, 0.40 and 0.43 for NP1, NP2 and NP3, respectively, suggesting that the drug release follows the Fickian diffusion mechanism.

3.4. Cytotoxicity of nanoparticles

The cytotoxicity of nanoparticles was accessed by CCK-8 assay. Fig. 4A showed the cell viability of MC3T3 cells incubated with nanoparticles at different concentrations (10–1000 μg mL^{-1}) for 24 h. Results showed that the cell viability was higher than 95% at all experimental concentration, indicating that the nanoparticles had no obvious cytotoxicity to MC3T3 cells and had good biocompatibility, which is suitable for the osteoporotic treatment. The cell viability increased over 100% at high nanoparticle concentrations (1000 μg mL^{-1}) in Fig. 4 could be an effect of the physical presence of particles, which increased the surface area available for cell growth [36]. According to previous report, the provision of a biocompatible environment in the vicinity of small cellular clusters could result in cell aggregation and an increase of proliferation rate in that area [37].

3.5. Celluar uptake

We further evaluated the specific cellular uptake of nanoparticles, and nanoparticles with or without Alen-decoration were incubated with HDF and MC3T3 cells for 3 and 24 h. Results showed that the amount of cellular uptake nanoparticles has little difference between NP4 (Alen-modified nanoparticles) and NP5 (nanoparticles without Alen-decoration) in both HDF and MC3T3 cells at 3 h, and the amount of cellular uptake nanoparticles increased in HDF and MC3T3 cells after 24 h incubation (Fig. 4B). It is noted that the amount of NP4 taken up by MC3T3 cells was significantly larger than that by HDF, whereas the amount of NP5 taken up by MC3T3 and HDF cells had no significant difference, revealing the specific cellular uptake of Alen-modified nanoparticles (NP4) by MC3T3, which might be caused by the preferential affinity between bisphosphonate (ex, Alen) and protein tyrosine phosphatases in osteoblasts [17].

Fig. 4C shows the confocal microscopy images of MC3T3 and HDF cells incubated with NP4 and NP5 for 3 h and 24 h. Very low fluorescence was observed in both MC3T3 and HDF cells incubated with NP4 and NP5 for 3 h, suggesting no preferential affinity between them. However, the fluorescence in MC3T3 cells incubated with NP4 for 24 h is

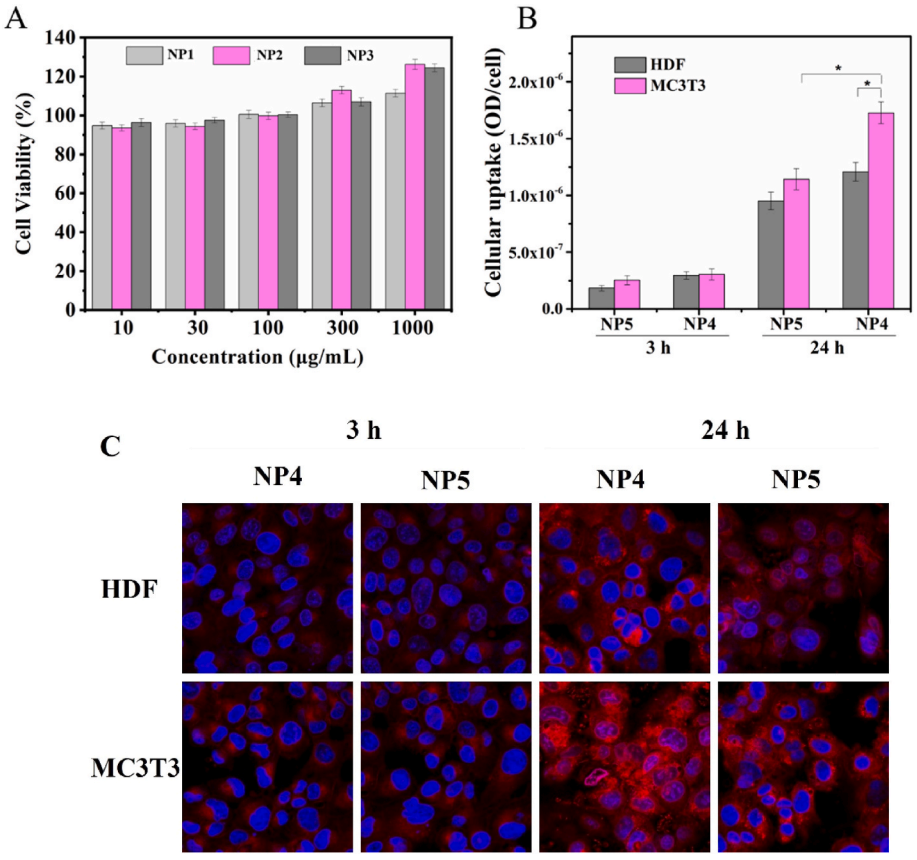

Fig. 4. (A) Cell viability of MC3T3 cells incubated with nanoparticles at different concentrations for 24 h. (B) Cellular uptake amount of NP4 (Alen-modified nanoparticles) and NP5 (nanoparticles without Alen-decoration) into HDF and MC3T3 cells after 3 and 24 h incubations. n = 5, $^*p < 0.05$. (C) Confocal microscopy images of HDF and MC3T3 cells incubated with NP4 and NP5 at 3 and 24 h. Nanoparticles were labeled using RB (red), and the cell nuclei were stained with DAPI (blue). (For interpretation of the references to colour in this figure legend, the reader is referred to the Web version of this article.)

remarkably more bright than that of other three (MC3T3 cells incubated with NP5, HDF cells incubated with NP4 and NP5), suggesting preferential affinity of NP4 (Alen-modified nanoparticles) to MC3T3. The fluorescence images matched to the corresponding results in Fig. 4B.

3.6. HAp affinity

As drug carriers for bone-targeting delivery, the bone affinity of nanoparticles is a very important property. Here, we investigated the affinity of nanoparticles to HAp, which is the main mineral component of bone. Fig. 5A showed the fluorescence images of HAp disks co-incubated with NP4 (Alen-modified nanoparticles) and NP5 (nanoparticles without Alen-decoration) at 0.5, 2 and 18 h. The fluorescence intensity of HAp disks increased with the incubation time, and HAp disks co-incubated with NP4 displayed more red fluorescence spot compared to that co-incubated with NP5. Quantified analysis of the fluorescence intensity using Image J demonstrated that the binding amount of NP4 to HAp disks was remarkably higher than that of NP5 at each test time point (Fig. 5B) including 0.5 h, which implied a rapid and stable binding of nanoparticles to HAp. The binding ratio of nanoparticles to HAp disks was also detected. As shown in Fig. 4c, the binding ratio of nanoparticles to HAp disks increased with the incubation time, and the binding ratio of NP4 to HAp disks was 17.8, 25.6 and 49.8% at 0.5, 2 and 18 h, respectively, which was apparently higher than that of NP5 (12.4, 20.1 and 42.4%). The stronger affinity of Alen-modified nanoparticles to HAp was contributed to the specific binding of Alen and Ca^{2+} in HAp (the main minerals of bone) [24], implying that the nanoparticulate system was feasible for bone-targeting delivery and had potential prospect for osteoporosis therapy.

4. Conclusion

Alen-modified nanoparticles prepared by CS-PLGA and Alen-PLGA were developed for bone-targeted delivery. The nanoparticles have an average size of 200–300 nm, and sustained drug release without obvious burst release can be observed. CCK-8 assay showed good cytocompatibility of the nanoparticles against MC3T3 cells. Cellular uptake of the nanoparticles revealed a specific cellular uptake of Alen-modified nanoparticles by osteoblasts (ex. MC3T3). HAp affinity test showed that the Alen-modified nanoparticles demonstrated a remarkable higher binding ratio to HAp disks than that of nanoparticles without Alen-decoration. Thus, this Alen-modified nanoparticle system showed

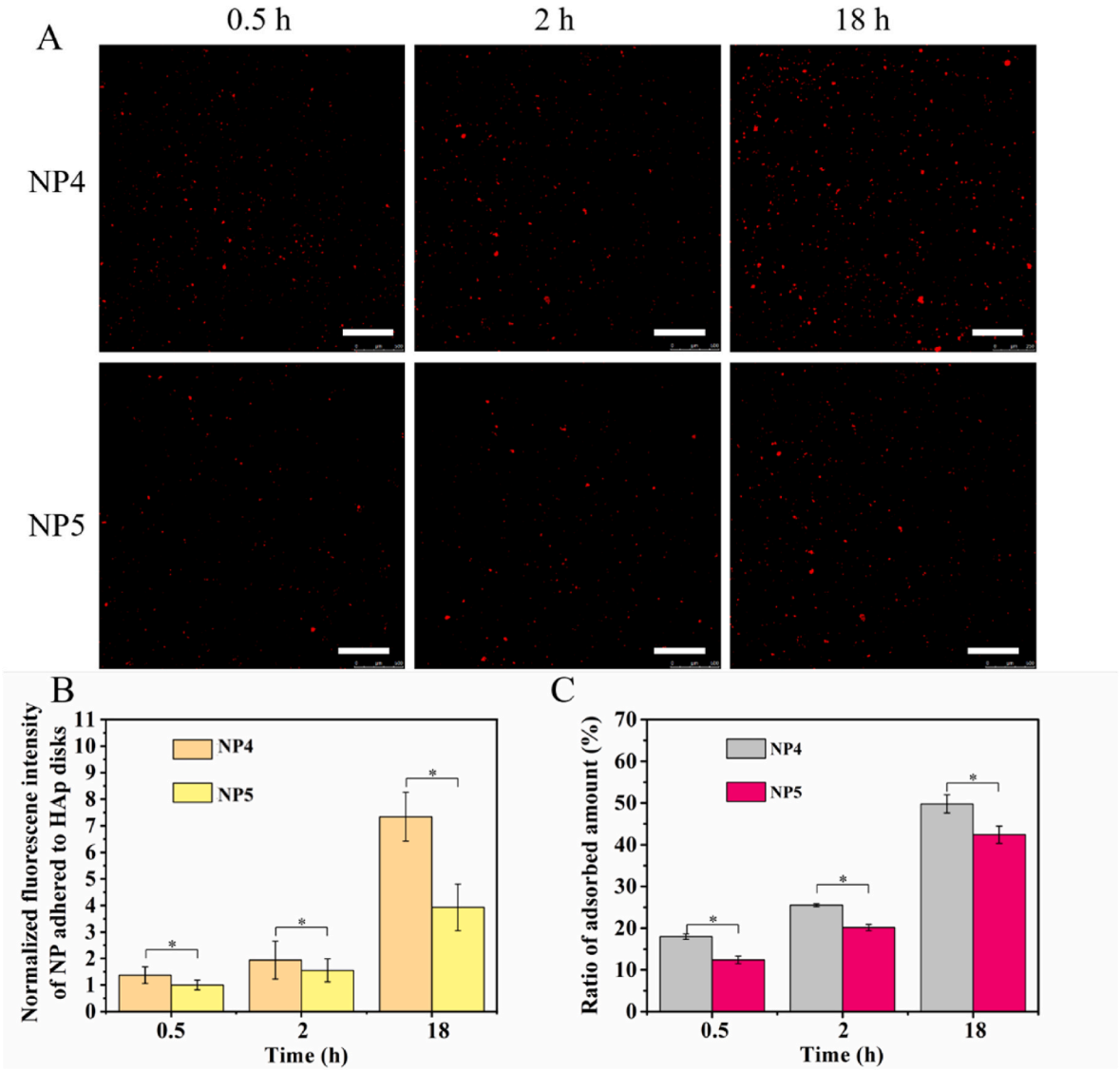

Fig. 5. (A) Fluorescence images of HAp disks co-incubated with NP4 (Alen-modified nanoparticles) and NP5 (nanoparticles without Alen-decoration) recorded by CLSM. (B) Quantification analysis of nanoparticles binding to HAp disks using Image J software. (C) Binding ratio of nanoparticles to HAp disks. n = 3, $*p < 0.05$. Scar bar = 500 μm.

potential promise in bone-targeted delivery for osteoporosis treatment.

CRediT authorship contribution statement

Chunlan Jing: Writing - Original Draft, Validation, Software, Formal analysis. **Shenmao Chen:** Validation, Formal analysis, Methodology. **Sehajdev Singh Bhatia:** Data curation. **Bowen Li:** Validation. **Hongze Liang:** Supervision. **Chaozong Liu:** Conceptualization, Resources. **Zhenjiang Liang:** Funding acquisition. **Junying Liu:** Funding acquisition. **Haiyan Li:** Funding acquisition. **Ziyu Liu:** Resources, Formal analysis. **Hui Tan:** Resources, Funding acquisition. **Lingling Zhao:** Conceptualization, Writing - Review & Editing, Investigation.

Declaration of competing interest

The authors declare that they have no known competing financial interests or personal relationships that could have appeared to influence the work reported in this paper.

Acknowledgement

This work was supported by the Basic scientific research operating expenses of provincial universities (grant number SJLY2021002); Science and Technology Innovation Commission of Shenzhen (grant number ZDSYS20200811142600003, JCYJ20180507183036060, JCYJ20190806161409092, JCYJ20210324103012033); Natural Science Foundation of Guangdong Province (grant number 2021A1515010720, 2019A1515011750); the K. C. Wong Magna Fund in Ningbo University; Key Laboratory of Advanced Mass Spectrometry and Molecular Analysis of Zhejiang Province; Versus Arthritis (grant number 21160 & 21977); and the European Commission via H2020-MSCA-RISE Program (grant number 734156).

References

[1] F. Baniahmad, S. Yousefi, M. Rabiee, S. Sara Shafiei, S. Faghihi, Alendronate sodium intercalation in layered double hydroxide/poly (ε-Caprolactone): application in osteoporosis treatment, Iran, J. Biotechnol. 19 (2021), e2490.
[2] G.Y. Ahn, S.E. Kim, T.H. Yun, I. Choi, D. Park, S.W. Choi, Enhanced osteogenic differentiation of alendronate-conjugated nanodiamonds for potential osteoporosis treatment, Biomater. Res. 25 (2021) 28.
[3] M. Frank, A. Grabos, A.G. Reisinger, D.B. Burr, D.H. Pahr, M.R. Allen, P.J. Thurner, Effects of anti-resorptive treatment on the material properties of individual canine trabeculae in cyclic tensile tests, Bone 150 (2021) 115995.
[4] M. Lorentzon, Treating osteoporosis to prevent fractures: current concepts and future developments, J. Intern. Med. 285 (2019) 381–394.
[5] J. Ye, J. Jiang, Z. Zhou, Z. Weng, Y. Xu, L. Liu, W. Zhang, Y. Yang, J. Luo, X. Wang, Near-infrared light and upconversion nanoparticle defined nitric oxide-based osteoporosis targeting therapy, ACS Nano 15 (2021) 13692–13702.
[6] S.J. Hwang, J.S. Lee, T.K. Ryu, R.H. Kang, K.Y. Jeong, D.R. Jun, J.M. Koh, S.E. Kim, S.W. Choi, Alendronate-modified hydroxyapatite nanoparticles for bone-specific dual delivery of drug and bone mineral, Macromol. Res. 24 (2016) 623–628.
[7] X. Xu, P. Zhang, X. Li, Y. Liang, K. Ouyang, J. Xiong, D. Wang, L. Duan, MicroRNA expression profiling in an ovariectomized rat model of postmenopausal osteoporosis before and after estrogen treatment, Am. J. Transl. Res. 12 (2020) 4251–4263.
[8] D. Li, J. Zhou, M. Zhang, Y. Ma, Y. Yang, X. Han, X. Wang, Long-term delivery of alendronate through an injectable tetra-PEG hydrogel to promote osteoporosis therapy, Biomater. Sci. 8 (2020) 3138–3146.
[9] K. Miladi, S. Sfar, H. Fessi, A. Elaissari, Enhancement of alendronate encapsulation in chitosan nanoparticles, J. Drug Deliv. Sci. Technol. 30 (2015) 391–396.
[10] Y. Cui, Z. Wang, Z. Li, X. Ji, B. Yuan, Y. Sun, C. Peng, Y. Leng, M. Dou, J. Wang, H. Liu, D. Wu, Functionalized anti-osteoporosis drug delivery system enhances osseointegration of an inorganic-organic bioactive interface in osteoporotic microenvironment, Mater. Des. 206 (2021) 109753.
[11] C.A. Martins, G. Leyhausen, J. Volk, W. Geurtsen, Effects of alendronate on osteoclast formation and activity in vitro, J. Endod. 41 (2015) 45–49.
[12] X. Gao, M. Guan, X. Liu, H.H.K. Xu, Q. Huang, L. Chen, S. Huang, Y. Xiao, X. Shi, Sustained delivery of growth factors and alendronate using partially demineralized dentin matrix for endogenous periodontal regeneration, Appl. Mater. Today 22 (2021) 100922.
[13] K. Miladi, S. Sfar, H. Fessi, A. Elaissari, Encapsulation of alendronate sodium by nanoprecipitation and double emulsion: from preparation to in vitro studies, Ind. Crop. Prod. 72 (2015) 24–33.
[14] Y. Zeng, J. Hoque, S. Varghese, Biomaterial-assisted local and systemic delivery of bioactive agents for bone repair, Acta Biomater. 93 (2019) 152–168.
[15] A. Qadir, Y. Gao, P. Suryaji, Y. Tian, X. Lin, K. Dang, S. Jiang, Y. Li, Z. Miao, A. Qian, Non-viral delivery system and targeted bone disease therapy, Int. J. Mol. Sci. 20 (2019) 565.
[16] H. Cheng, A. Chawla, Y. Yang, Y. Li, J. Zhang, H.L. Jang, A. Khademhosseini, Development of nanomaterials for bone-targeted drug delivery, Drug Discov. Today 22 (2017) 1336–1350.
[17] T.K. Ryu, R.H. Kang, K.Y. Jeong, D.R. Jun, J.M. Koh, D. Kim, S.K. Bae, S.W. Choi, Bone-targeted delivery of nanodiamond-based drug carriers conjugated with alendronate for potential osteoporosis treatment, J. Contr. Release 232 (2016) 152–160.
[18] Z. Zhou, T. Fan, Y. Yan, S. Zhang, Y. Zhou, H. Deng, X. Cai, J. Xiao, D. Song, Q. Zhang, Y. Cheng, One stone with two birds: phytic acid-capped platinum nanoparticles for targeted combination therapy of bone tumors, Biomaterials 194 (2019) 130–138.
[19] K.B. Farrell, A. Karpeisky, D.H. Thamm, S. Zinnen, Bisphosphonate conjugation for bone specific drug targeting, Bone Rep. 9 (2018) 47–60.
[20] M.G. Arafa, H.A. Mousa, N.N. Afifi, Preparation of PLGA-chitosan based nanocarriers for enhancing antibacterial effect of ciprofloxacin in root canal infection, Drug Deliv. 27 (2020) 26–39.
[21] E. Manek, F. Darvas, G.A. Petroianu, Use of biodegradable, chitosan-based nanoparticles in the treatment of alzheimer's disease, Molecules 25 (2020) 4866.
[22] C.K. Thakur, N. Thotakura, R. Kumar, P. Kumar, B. Singh, D. Chitkara, K. Raza, Chitosan-modified PLGA polymeric nanocarriers with better delivery potential for tamoxifen, Int. J. Biol. Macromol. 93 (2016) 381–389.
[23] W. Xu, R. Zhao, T. Wu, G. Li, K. Wei, L. Wang, Biodegradable calcium carbonate/mesoporous silica/poly(lactic-glycolic acid) microspheres scaffolds with osteogenesis ability for bone regeneration, RSC Adv. 11 (2021) 5055–5064.
[24] C. Jing, H. Tan, C. Zhang, H. Liang, H. Na, S. Chen, C. Liu, L. Zhao, Alendronate-decorated nanoparticles as bone-targeted alendronate carriers for potential osteoporosis treatment, ACS Appl. Bio Mater. 4 (2021) 4907–4916.
[25] L. Zhao, L. Zhu, Q. Wang, J. Li, C. Zhang, J. Liu, X. Qu, G. He, Y. Lu, Z. Yang, Synthesis of composite microgel capsules by ultrasonic spray combined with in situ crosslinking, Soft Matter 7 (2011) 6144–6150.
[26] Z. Wu, S. Zhang, X. Zhang, S. Shu, T. Chu, D. Yu, Phenylboronic acid grafted chitosan as a glucose-sensitive vehicle for controlled insulin release, J. Pharmaceut. Sci. 100 (2011) 2278–2286.
[27] H. Murakami, M. Kobayashi, H. Takeuchi, Y. Kawashima, Utilization of poly(DL-lactide-co-glycolide) nanoparticles for preparation of mini-depot tablets by direct compression, J. Contr. Release 67 (2000) 29–36.
[28] R. Pignatello, E. Cenni, D. Micieli, C. Fotia, M. Salerno, D. Granchi, S. Avnet, M. G. Sarpietro, F. Castelli, N. Baldini, A novel biomaterial for osteotropic drug nonocarriers synthesis and biocompatibility evaluation of a PLGA-ALE conjugate, Nanomedicine-UK 4 (2009) 161–175.
[29] F.F. Azhar, A. Olad, A study on sustained release formulations for oral delivery of 5-fluorouracil based on alginate-chitosan/montmorillonite nanocomposite systems, Appl. Clay Sci. 101 (2014) 288–296.
[30] Y. Yang, Y. Liu, S. Chen, K.L. Cheong, B. Teng, Carboxymethyl β-cyclodextrin grafted carboxymethyl chitosan hydrogel-based microparticles for oral insulin delivery, Carbohydr. Polym. 246 (2020) 116617.
[31] J. Zhang, Y. Liu, R. Luo, S. Chen, X. Li, S. Yuan, J. Wang, N. Huang, In vitro hemocompatibility and cytocompatibility of dexamethasone-eluting PLGA stent coatings, Appl. Surf. Sci. 328 (2015) 154–162.
[32] Z. Yuan, P. Wei, Y. Huang, W. Zhang, F. Chen, X. Zhang, J. Mao, D. Chen, Q. Cai, X. Yang, Injectable PLGA microspheres with tunable magnesium ion release for promoting bone regeneration, Acta Biomater. 85 (2019) 294–309.
[33] J. Li, Y. Zhang, H. Tan, X. Yan, L. Zhao, H. Liang, pH and glucose dually responsive injectable hydrogel prepared by in situ crosslinking of phenylboronic modified chitosan and oxidized dextran, J. Polym. Sci., Polym. Chem. Ed. 53 (2015) 1235–1244.
[34] R. Vinay, V. KusumDevi, Potential of targeted drug delivery system for the treatment of bone metastasis, Drug Deliv. 23 (2016) 21–29.
[35] Y. Cong, C. Quan, M. Liu, J. Liu, G. Huang, G. Tong, Y. Yin, C. Zhang, Q. Jiang, Alendronate-decorated biodegradable polymeric micelles for potential bone-targeted delivery of vancomycin, J. Biomater. Sci. Polym. Ed. 26 (2015) 629–643.
[36] S.S.H. Matrali, A.K. Ghag, Feedback-controlled release of alendronate from composite microparticles, J. Funct. Biomater. 11 (2020) 46.
[37] B. Fu, X. Sun, W. Qian, Y. Shen, R. Chen, M. Hannig, Evidence of chemical bonding to hydroxyapatite by phosphoric acid esters, Biomaterials 26 (2005) 5104–5110.